International Journal of Environmental Science and Technology (2023) 20:859–870
https://doi.org/10.1007/s13762-022-04004-2

ORIGINAL PAPER

Removal of 3-chlorocarbazole using a Fe/Ni bimetallic nanocomposite as an effective catalyst: characteristics and mechanism

X. Kang[1] · D. Li[2] · L. Chu[3] · X. Zhao[1] · X. Song[4] · X. Cao[5,6]

Received: 27 April 2021 / Revised: 10 September 2021 / Accepted: 30 January 2022 / Published online: 28 February 2022

Abstract

Halogenated carbazoles have become a new type of contaminant due to their persistence, teratogenicity and toxicity. A bimetallic nanoparticle material containing Fe/Ni is used to remove 3-chlorocarbazole in aqueous solution. The surface morphology of Fe/Ni was studied using scanning electron microscopy, X-ray diffraction and X-ray photoelectron spectrometer as characterization methods. From the batch experiment, it became clear that the iron–nickel ratio, pH, temperature and catalyst dosage are key factors, which affect the removal of 3-chlorocarbazole. The kinetic fitting shows that a pseudo-first-order kinetic model can be used to describe the removal process of 3-chlorocarbazole. Using various techniques, the mechanism of cooperative adsorption and catalytic reduction of Fe/Ni to remove 3-chlorocarbazole was studied. The high-pressure liquid chromatography analysis results show that the dechlorination product of 3-chlorocarbazole is carbazole.

Graphical abstract

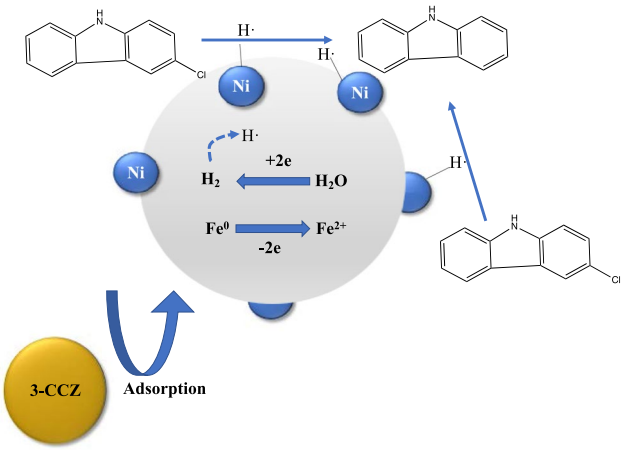

Keywords 3-chlorocarbazole · Dechlorination · Fe/Ni nanoparticles · Kinetics · Removal

Introduction

Polyhalogenated carbazoles (PHCZs) are well-known emerging environmental pollutants. In view of their wide distribution in the environment and their structural similarity with dioxins and dioxin-like chemicals (DLC), their environmental behavior and ecological risk have become a major concern for governments and scientists. In the past few decades, more and more PHCZs have been found in

Editorial responsibility: Gaurav Sharma.

✉ X. Zhao
zxx@dhu.edu.cn

Extended author information available on the last page of the article

air, water, dust, fish, sediments and soils of North America, Europe and Asia (Wu et al. 2017, 2018; Zhu and Hites 2006). Especially, for China 3-chlorocarbazole (3-CCZ) has been detected often in the surface sediments of the Yellow River, the northern South China Sea and the Sanmen Bay of the East China Sea (Li et al. 2020b; Qiu et al. 2019a; Zhou et al. 2020). At present, there is relatively few research available on the concentration and on the evaluation of PHCZs in the aquatic environment. Wang et al. (2019) collected 10 tap water samples from a pressurized water treatment plant in Wuhan, of which 9 samples were detected with PHCZs, with a total concentration of 3.6–51.9 ng/L. Li et al. (2020a) detected 5 PHCZs in the surface water of the Yellow Sea with concentrations of 0.062–0.322 ng/L. The top three substances were 3,6-BCZ (0.010–0.682 ng/L), 3,6-CCZ (0.035–0.269 ng/L) and 3-CCZ (0.010–0.020 ng/L) (Li et al. 2020). Since these are toxic substances, it is necessary to investigate the mechanism of PHCZs in water bodies.

In the past few years, various methods for removal of PHCZs have been studied extensively. These include physical adsorption, microbial degradation and chemical degradation. But the effectiveness of the adsorption method is generally insufficient, because the structure of the pollutants cannot be destroyed fundamentally (Qiu et al. 2019b; Xiaojun et al. 2019). There are reports on the microbial degradation of 3-BCZ (3-bromocarbazole) (Ma et al. 2017), but the microbial degradation has the disadvantage of needing a long time remove, which means a low degradation rate (Ma et al. 2017). The process of direct photolysis can remove the halogen atoms from PHCZs in the presence of a hydrogen donor. The photochemical degradation of PHCZs has confirmed that the stepwise reduction by debromination is one of the mechanisms of bromination and mixed halogenation (containing bromine and chlorine) carbazole (Pan et al. 2019; Shanshan et al. 2019). Advanced oxidation methods (AOPs) have been proven to be effective to degrade pollutants, because reactive oxygen species (ROS) are involved. According to ROS formation and reaction conditions, AOPs include Fenton reaction, photocatalytic oxidation, piezoelectric catalysis, etc. Meanwhile, it has been widely used for the degradation of various organic compounds and dyes. For example, Lu et al. (2021) studied Ag/Bi_5O_7I nanocomposite firstly for piezo/photocatalytic reduction of N_2 to NH_3 and methyl orange (MO) degradation (Lu et al. 2021). Feng et al. (2020) studied the in situ preparation of the g-C_3N_4/$Bi_4O_5I_2$ complex and its photoactivity to degrade methyl orange under visible light (Feng et al. 2020). Cheng et al. (2021) studied the degradation of dyes by HT-Bi_2MoO_6 microspheres (Cheng et al. 2021). Among them, a solid-phase Fenton catalysis can degrade efficiently many refractory organics, but the reaction requires an extremely high pH and easily produces Fe sludge (Bokare et al. 2008; Nidheesh and Gandhimathi 2012; Xi et al. 2014).

Due to its large specific surface area, nano-zero-valent iron (nZVI) has a high reactivity. In the past ten years, it has been used widely to degrade various organic compounds (Ghauch et al. 2009; Su et al. 2011; Yin et al. 2012). But at the same time there is also the disadvantage of easy agglomeration and reduced reactivity. To enhance the reactivity of nZVI, generally a second catalytic metal like Pd, Ag, Cu, Al, Ni, etc., is added to improve the stability of the reaction (Ruan et al. 2019). Gao et al. studied the degradation of microcystin by Fe/Pd and Fe/Ni catalysts. They found that Fe^0 reacts with microcystin and is oxidized to iron oxide or hydroxide. Ni or Pd acts as catalyst to prevent Fe^0 from corroding and acts with water to produce hydrogen (Gao et al. 2016). Although the catalytic effect of Ni is weaker than that of Pd, its improved corrosion stability and reduced cost may make it more suitable for on-site repair and wastewater treatment (Theron et al. 2008). Ni bimetallic nanoparticles enable nZVI to suppress air by inhibiting oxidation and increasing reactivity. In order to achieve this goal, we introduce a second catalytic metal like Ni into nZVI to form bimetallic nanoparticles. However, for the characteristics and mechanism of PHCZs removal by Fe/Ni bimetals little information is available.

In this study, nano-bimetallic Fe/Ni particles were synthesized to remove 3-CCZ from aqueous solution. For this purpose, scanning electron microscopy (SEM), X-ray diffraction (XRD) and X-ray photoelectron spectrometer (XPS) were used to characterize the Fe/Ni particles. Also, the best iron–nickel mass ratio of the catalyst for the 3-CCZ removal was determined. The effects of pH, material dosage, and temperature on the removal effect were explored. Kinetic fitting and E_a calculation of Fe/Ni removal process were performed. From the products, the degradation mechanism of 3-CCZ was deduced by HPLC, GC–MS, IC and CNS. Finally, experiments were carried out on the recycling possibility of the Fe/Ni materials.

All experiments were conducted in the School of Environment, Donghua University (Shanghai, China). The experiments were performed from June to September 2020.

Materials and methods

Materials and chemicals

Ferrous sulfate ($FeSO_4·7H_2O$, 97%), nickel (II) sulfate hexahydrate ($NiSO_4·6H2O \geq 98\%$), hydrochloric acid (HCl, 35%), ethanol (≥ 99.5), sodium hydroxide ($NaOH \geq 98\%$) and sodium borohydride ($NaBH_4 \geq 98\%$) were purchased from Sinopharm Chemical Reagent Co., Ltd., Shanghai, China. 3-Chlorocarbazole (3-CCZ, ≥ 99%) was purchased from Sigma-Aldrich. Deionised water was supplied by

Donghua University. All chemicals were of analytical reagent grade.

Synthesis of Fe/Ni

Fe/Ni particles were synthesized by a chemical reduction method. The method of preparing ferrous sulfate and nickel sulfate from sodium borohydride has been described by (Chen et al. 2011). Briefly, 10.00 g of $FeSO_4{\cdot}7H_2O$ and 1.80 g $NiSO_4{\cdot}6H_2O$ are suspended in a mixture of 25 mL water and 75 mL absolute ethanol and then stirred for 20 min under a N_2 atmosphere. Then, 1.0 M $NaBH_4$ solution is prepared by adding 3.78 g of $NaBH_4$ to 100 mL of deoxygenated deionized water. The solution is added drop by drop to the slurry mixture of the bimetallics. Fe^0 and Ni^0 nanoparticles are prepared by the reactions shown in Eqs. (1) and (2) (Mukherjee et al. 2011; Zhao et al. 2014):

$$2Fe^{2+} + BH^- + 2H_2O \rightarrow 2Fe^0 \downarrow + BO_2^- + 4H^+ + 2H_2 \uparrow \quad (1)$$

$$Ni^{2+} + 2BH_4^- + 6H_2O \rightarrow Ni^0 \downarrow + 2B(OH)_3 + 7H_2 \uparrow \quad (2)$$

After stirring for 2 h, the product is separated by vacuum filtration, washed 3 times with 600 mL of absolute ethanol, and then dried in a vacuum freeze dryer. The tailored product is denoted as "Fe/Ni."

Sample characterization

The morphological analysis of "Fe/Ni" was performed using a scanning electron microscope (SEM, Zeiss Sigma 500, Germany). The X-ray diffraction (XRD) spectra of "Fe/Ni" were obtained with a powder X-ray diffractometer (D/max-2550 PC, Japan) working with Cu–Ka (l ¼ 0.154 nm) radiation generated at 40 kV and 40 mA with a scan rate of 3° 2θ per minute from 5 to 70° 2θ. The X-ray photoelectron spectrometry (XPS) analysis of Fe/Ni was done utilizing XPS (Escalab 250Xi).

Analytical methods

3-CCZ concentrations were measured by high-pressure liquid chromatography (HPLC) (Thermo Fisher, USA). The HPLC conditions were: mobile phase acetonitrile: water (80:20, V/V), analytical column Grace Alltima C_{18} column (4.6 mm × 250 mm, 5 µm), detection wavelength 345 nm, flow rate 1.0 mL/min, injection volume 20 µL and the column temperature 25 °C.

The removal efficiency for antibiotics using Fe/Ni nanoparticles is estimated by the following equation:

$$R(\%) = \frac{c_0 - c_t}{c_0} \times 100\% \quad (3)$$

where R (%) represents the removal efficiency of 3-CCZ and C_0 (mg/L) and C_t (mg/L) are the initial concentration and the concentration at t (min) of 3-CCZ in aqueous solution.

The degradation products of 3-CCZ were detected by GC–MS (GCMS-QP2010Ultra, USA), chromatographic column DB-5 MS capillary column (30 m × 0.32 mm × 0.25 µm) carrier gas high-purity helium. Temperature rising procedure: Initial temperature 80 °C is kept for 3 min, increases to 150 °C at 10 °C/min, then raises to 250 °C at 5 °C/min; keep for 10 min and finally raise it to 300 °C at 5 °C/min and keep for 10 min. Carrier gas flow rate: 1.2 mL/min. The temperatures inlet for oven, quadrupole, and ion source were 280, 80, 150 and 230 °C, respectively. Injection mode: splitless; injection volume: 2 µL; ion source: EI source.

The Cl^- concentration was determined by ion chromatography (Thermo Fisher, USA) with an eluent of 15 mmol/L KOH. The injection volume is 20 µl, and the flow rate is 1.0 mL/min.

Elemental analysis (CNS) was performed using LECO TRUMAC CNS analyzer. The samples were heated to 1300 °C in a furnace with 20 s dehydration time in the presence of helium, oxygen and nitrogen.

Batch experiments for 3-CCZ removal

At first, the optimal iron–nickel ratio of the catalyst was determined. Fe/Ni materials with m (Fe/Ni) of 2:1, 3:1, 5:1 and 10:1 were prepared. The reaction was carried out at a temperature of 30 °C, pH = 7.0 and a material dosage of 2.0 g/L to determine the best iron–nickel ratio. Then, 0.2 g "Fe/Ni" material was weighed in 100 mL reaction solution containing 25% ethanol as a co-solvent and 5 mg/L 3-CCZ. Anaerobic water was used. Except for the experiment of the amount of catalyst, the concentration of Fe was kept always at 2 g/L. In the pH experiment the solution was kept at 7.0, temperature at 30 °C and 200 rpm/min. Supernatants were withdrawn with 0.45 µm hydrophilic PTFE syringe filters. The 3-CCZ concentration was measured by HPLC. After determining the 3-CCZ concentration, the removal efficiency was calculated using Eq. (3).

Various experimental parameters may affect the efficiency of the Fe/Ni particles for degrading 3-CCZ in aqueous solution. The pH used in this experiment (4.0, 7.0, 10.0) had been adjusted with concentrated hydrochloric acid/sodium hydroxide (1 mol/L). The doses of "Fe/Ni" were 1.0, 2.0, 4.0 and 8.0 g/L. The reaction temperatures were 20, 30 and 40 °C. The initial concentration of 3-CCZ was always 5 mg/L. In addition, the reuse of "Fe/Ni" for the 3-CCZ removal was evaluated. A 3-CCZ solution (100 mL) of 0.2 g "Fe/Ni" at 5 mg/L was added. After 7 h the solution was

centrifuged at 3000 r/min for 10 min to obtain a solid–liquid separation. The "Fe/Ni" was reused to remove new 3-CCZ solution 3 times in a row. All experiments were performed in triplicate.

Kinetics of 3-CCZ removal

Since the removal of 3-CCZ is generally regarded as occurring at the surface of "Fe/Ni," the removal rate depends mainly on the available surface area (Bokare et al. 2008). The removal kinetics is expressed as a pseudo-first-order equation as shown below:

$$\ln\frac{c}{c_0} = -k_{\text{obs}}t \tag{4}$$

where k_{obs} is the observed rate constant of a pseudo-first-order reaction (/min) and can be calculated from the slope of the line by plotting ln (c/c_0) versus t (/min).

The apparent activation energy E_a is calculated from the Arrhenius equation (Bokare et al. 2008; Zhang et al. 2011):

$$\ln k_{\text{obs}} = -\frac{E_a}{RT} + \ln A_0 \tag{5}$$

where E_a (kJ/mol) is the apparent activation energy and A_0 is a pre-exponential factor with the same dimension as k_{obs}.

Results and discussion

Characterization

To explore the surface morphology of the nanomaterial "Fe/Ni," a SEM was used to observe the particle size and morphological changes of freshly prepared "Fe/Ni." As shown in Fig. 1a, b, under different magnification, the structure of freshly prepared Fe/Ni is displayed. The nano-Fe/Ni has a porous morphology. This indicates that they are prone to aggregate under the action of magnetism. For this reason, it is easy to adsorb and degrade pollutants. Figure 1c, d shows the Fe/Ni after reaction. Figure 1c, d shows the rough surface

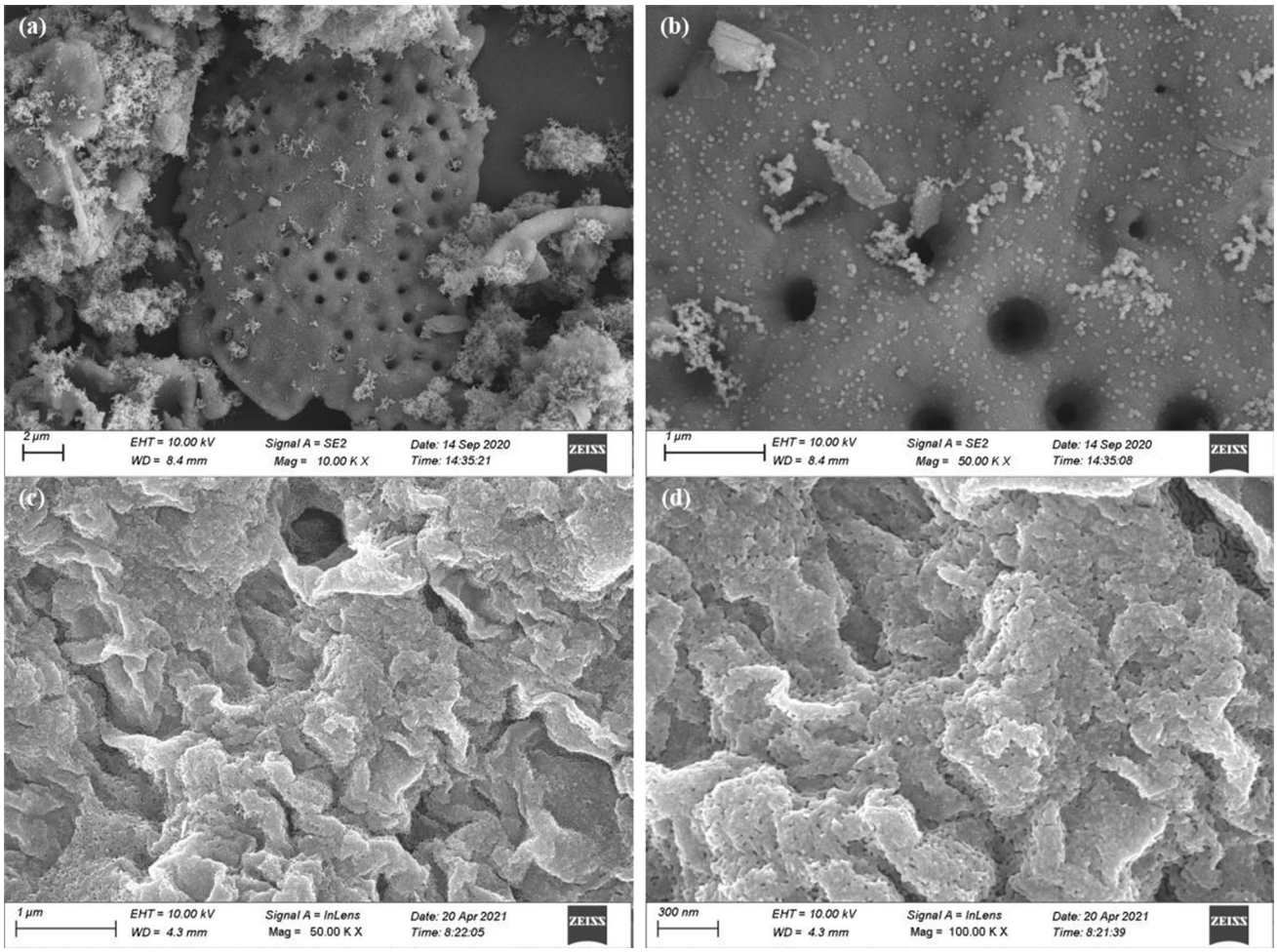

Fig. 1 SEM images of freshly prepared and reacted Fe/Ni particles. **a, b** SEM of freshly prepared Fe/Ni **c**, **d** SEM of reacted Fe/Ni

of the material. This is due to the removal of 3-CCZ resulting in the formation of an iron oxide layer. For example, the passivation of the nZVI surface caused iron oxide (Liu et al. 2013), which was also verified by our XRD analysis.

The XRD patterns of freshly prepared Fe/Ni and reacted Fe/Ni are shown in Fig. 2. As shown in Fig. 2a, the significant characteristic peak of $2\theta = 44.8°$ illustrates the crystallization of Fe^0 in Fe/Ni (Fang et al. 2011; Lin et al. 2012). A nickel signal was detected at ($2\theta = 44.5°$), but is not visible significantly because of its extremely low fraction (0.5 wt%) at the particle surface. After the reaction of Fe/Ni with 3-CCZ, the iron oxide formed is shown in Fig. 2b, where Fe_3O_4 is found at $2\theta = 35.5$, and Fe_2O_3 at $2\theta = 30.3$ (Su et al. 2011). In addition, a decrease in the apparent peak of Fe^0 was observed. It can be concluded that iron acts as a redox agent in the removal of 3-CCZ (Weng et al. 2014a; Su et al. 2011).

XPS was used to further determine the elemental composition and chemical oxidation state of freshly prepared Fe/Ni, as shown in Fig. 3. XPS revealed the two elements Fe and Ni. Peaks are visible at 706.8 eV (Fe^0 $2p^{3/2}$) and 719.4 (Fe^0 $2p^{1/2}$), indicating the presence of Fe^0 in Fe/Ni. The peaks at 710.8 eV and 724.2 eV are characteristic peaks for Fe3p2$p^{3/2}$ and Fe2p $2p^{1/2}$, respectively. This confirms that the surface of Fe/Ni is formed by a layer of oxides due to the synthesis of Fe/Ni (Fang et al. 2011). In Fig. 3d, the XPS spectrum of Ni $2p^{3/2}$ displays a peak at 855.1 eV, which indicates the occurrence of Ni^{2+}. Moreover, a peak at 852.4 eV

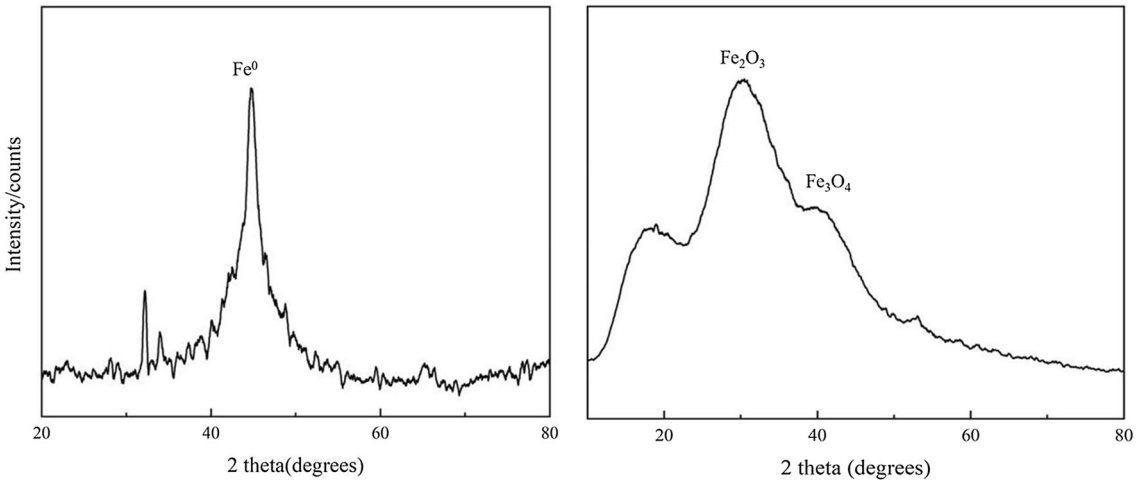

Fig. 2 XRD patterns **a** freshly prepared Fe/Ni; **b** after reacted Fe/Ni

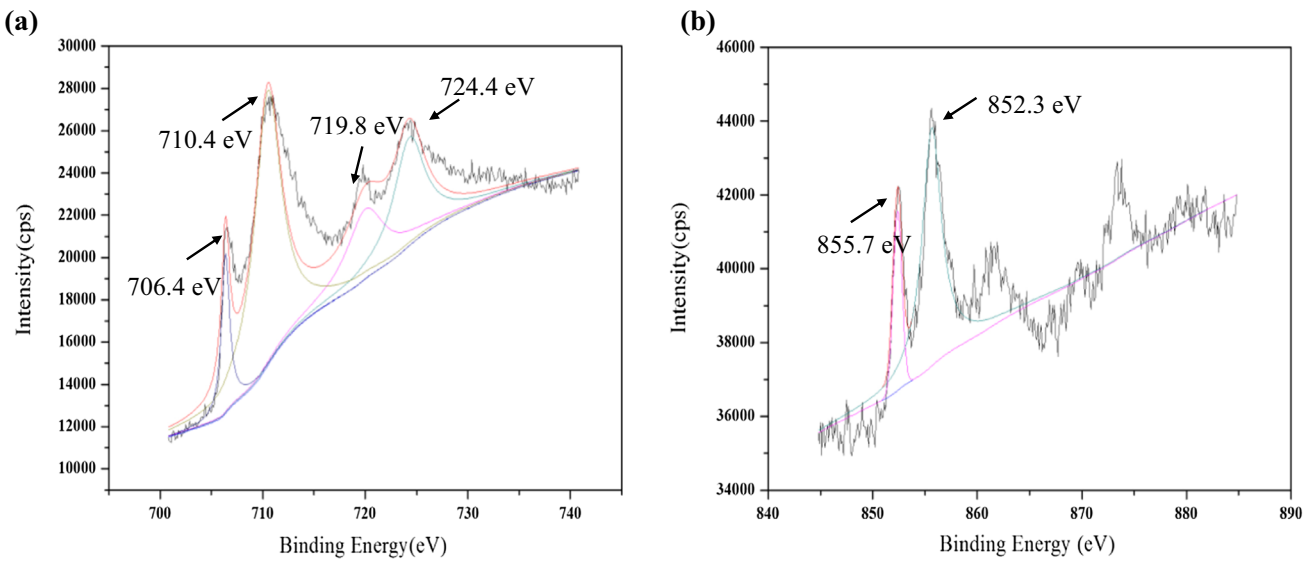

Fig. 3 XPS spectra of freshly prepared Fe/Ni: **a** Fe_{2p}. **b** Ni_{2p}

can be attributed to Ni^0. Thus, the XPS data show that in the nanoparticles Fe and Ni exist in different valence states at the surface.

Batch removal experiments of 3-CCZ

Effect of Fe/Ni mass ratio

In order to determine the best iron-to-nickel ratio in the catalyst, the impact of Fe/Ni mass ratio on the removal of 3-CCZ by Fe/Ni was investigated. Particles with n(Fe): n(Ni) of 2:1, 3:1, 5:1 and 10:1 were tested. The results are shown in Fig. 4a. If the relative content of Ni increases from 10:1 to 2:1, the removal of 3-CCZ at first increases and then decreases. This can be explained as follows. This is a consequence in bimetallic system, nZVI acts as a reducing agent, whereas the other metal such as Ni was the function of a hydrogenation catalyst. Furthermore, the presence of Ni also disperses the iron particles, which enhances the corrosion of these particles and, thus, increases the removal efficiency (Ezzatahmadi et al. 2016; Fu et al. 2014). With the increase of Fe^0 contents the amount of 3-CCZ removal increases due to the reducing rose. If the Fe^0 amount increased, furthermore the percentage of Ni in Fe/Ni decreases causing the effect of Ni to decrease, which causes the Fe^0 reduction ability to reach saturation. In addition, considering that the ratio of Fe/Ni 5:1 has the best effect, so 5:1 was selected to further study.

Effect of pH

The pH for the removal of 3-CCZ by the Fe/Ni catalyst was tested at pH 4.0, 7.0 and 10.0. The results are shown in Fig. 4b. When pH increased from 4.0 to 10.0, the 3-CCZ removal efficiency decreases with the increase of pH from 4.0 to 10.0 after 1 h. After 3 h, the 3-CCZ removal efficiency nearly reached 100% at pH 4.0 and 7.0, which higher than pH 10.0. This further indicates that pH 4.0 and 7.0 are more

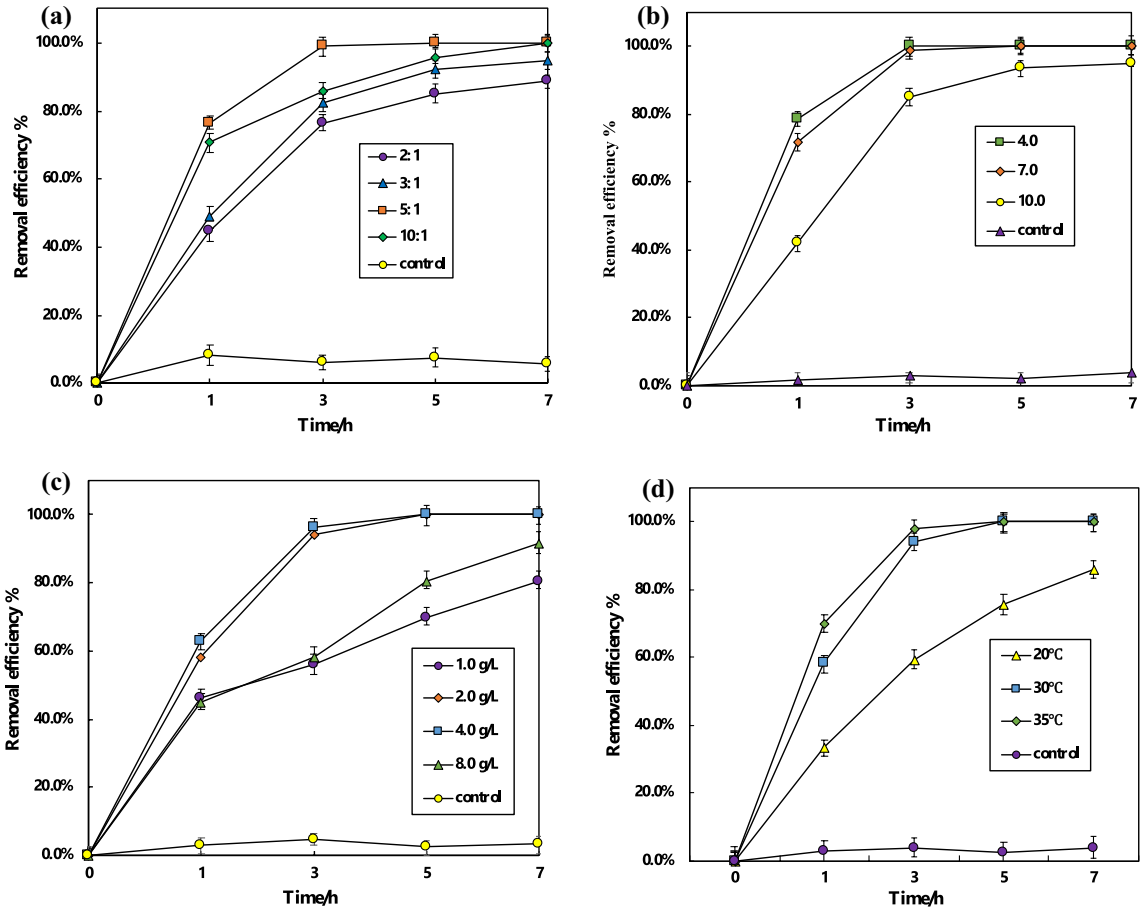

Fig. 4 Removal of 3-CCZ under different conditions. **a** Influence of different Fe/Ni mass ratios: 100 mL; C_0 = 5 mg/L; 30 °C; Fe/Ni dosage: 2.0 g/L; pH = 7.0 Fe–Ni ratio 2:1, 3:1, 5:1, 10:1 **b** Effect of different initial pH: 100 mL; C_0 = 5 mg/L; 30 °C; amount of Fe/Ni: 2.0 g/L; pH = 4.0, 7.0, 10.0; hypoxic conditions under. **c** Different dosages of Fe/Ni: 100 mL; C_0 = 5 mg/L; 30 °C; Fe/Ni dosage: 1.0 g/L, 2.0 g/L, 4.0 g/L, 8.0 g/L; pH = 7.0; hypoxic conditions. **d** Different temperatures. Conditions: 100 mL; C_0 = 5 mg/L; 20 °C, 30 °C, 35 °C; Fe/Ni dosage: 2.0 g/L; pH = 7.0; hypoxic conditions

favorable than pH 10.0 for a removal of 3-CCZ. Generally, a low pH is conducive to the corrosion of iron in an aqueous environment. The corrosion of Fe is beneficial to the formation of atomic hydrogen on the surface of Ni, followed by a formation of molecular hydrogen (Bokare et al. 2008). On the contrary, under alkaline condition, a slow generation of hydrogen limits the removal of 3-CCZ. Therefore, when pH increased from 4.0 and 7.0 to 10.0, the corrosion of Fe becomes slow, causing the amount of atomic hydrogen on the Ni surface to be low too. The amount of hydrogen radicals generated limit the removal efficiency of 3-CCZ by Fe/Ni catalyst. Furthermore, the precipitation of metal hydroxides on the catalyst surface forms a passivation layer, which can also deactivate the Fe/Ni bimetallic nanoparticles (Zhou et al. 2010). Therefore, an optimal removal of 3-CCZ from water by the Fe/Ni catalyst is obtained under acidic conditions.

It can be seen from Fig. 4b that between 3 and 7 h, the removal of 3-CCZ at pH 4.0 was similar to the one at pH 7.0. Thus, this type of reaction is better than the ordinary Fenton reaction, although it uses hydrogen radicals to oxidize and degrade pollutants (Bokare et al. 2008; Weng et al. 2014a). Unlike the Fenton reaction, which is effective in the pH range of 2.0–3.0, this process shows the ability to remove 3-CCZ at neutral pH (~ 6.72). More important, hydrogen peroxide (H_2O_2) is needed to start the Fenton reaction, but this reaction here does not need H_2O_2. On the other hand, similar to the Fenton reaction, which is usually carried out at pH 3.0, this type of AOP is carried out also at pH 3.0 to maintain the iron species in solution. It requires downstream processing to increase the pH and precipitate the catalyst as hydroxide iron. Based on the data shown above, pH 7.0 was selected for the further study.

Effect of Fe/Ni dosage

Figure 4c shows the effect of Fe/Ni dosage on the removal of 3-CCZ. The data in Fig. 4c show that if the dosage of "Fe/Ni" is increased from 1.0 to 2.0 g/L, the removal efficiency of 3-CCZ increases significantly too. With an increased Fe/Ni dosage, the amount of reactive sites increases also, resulting in the improvement of the reaction efficiency. This is accordance with results observed in studies of Fe/Ni used to remove 2,4-DCP and AMX (Ezzatahmadi et al. 2019; Weng et al. 2014b). However, a further increase of the catalyst from 2.0 to 4.0 g/L did not cause any improved removal of 3-CCZ. The removal even decreased, if the catalyst amount further increased to 8.0 g/L. The low 3-CCZ removal efficiency of Fe/Ni at a dosage of 8.0 g/L can be due to the fact that the increased dosage caused the pH of the solution to increase. This in turn may have led to a formation of iron oxides, which caused a reduced removal of 3-CCZ (Ezzatahmadi et al. 2019). Considering that the removal of 3-CCZ at dosage 2.0 g/L and 4.0 g/L were higher than those at dosage of 1.0 g/L, so 2.0 g/L were chosen as the optimal dosage of Fe/Ni for further experiment.

Effect of temperature

To assess the effect of different temperatures, experiments were carried out at 20, 30 and 35 °C. The results are shown in Fig. 4d. As shown in Fig. 4d, when the reaction time was increased from 1 to 3 h, the removal efficiency of 3-CCZ increased if the temperature was increased from 20 to 35 °C. If the reaction time was further increased to 5 h, the removal of 3-CCZ at 30 °C and 35 °C reached 100%, which was significantly higher than 20 °C. This shows that increasing the temperature causes an improved removal of 3-CCZ. This is probably an effect of temperature causing an increasing rate of migration of 3-CCZ particles from the liquid phase to the surface of the nanoparticles (Liu et al. 2013), where they can be removed.

The removal mediated by Fe/Ni nano-bimetals occurs mostly with surface adsorbed compounds. The effect of the temperature on the removal is shown in Fig. 4d. As the temperature was increased from 20 to 30 °C, the removal efficiency also increased significantly. This may have been caused by two factors: firstly, at increased temperature the mobility of 3-CCZ from solution to the surfaces of the nanoparticles may cause increased adsorption. This is consistent with the results of Zhang et al. on 2,4-DCP removal (Zhang et al. 2009). Secondly, the increased temperature was selected provides enough energy (Dong et al. 2011). Based on the findings, 30 °C was selected as the optimal removal temperature.

In order to explore, whether the optimal 3-CCZ removal conditions are suitable also for the use of tap water, the optimal conditions ($C_0 = 5$ mg/L; 30 °C; Fe/Ni dosage: 2.0 g/L; pH = 7.0 Fe–Ni ratio 5:1) were used to compare the differences in the removal rates for 3-CCZ between ultrapure and tap water. As shown in Table 1, there is no significant difference in the removal of 3-CCZ for the two types of water. It means, that the catalyst can be used also with tap water systems.

Table 1 The removal rate of 3-CCZ in different water bodies

Different water conditions	Removal rate of 3-CCZ (%)	Time (h)
Tap water	100	5
Ultrapure water	100	5

Control experiment

In order to evaluate the synergistic effect between Fe and Ni in the catalyst, three control experiments including (a) Fe/Ni, (b) Fe^0 and (c) Ni were arranged to deal with 3-CCZ in aqueous solution under the optimal conditions ($C_0 = 5$ mg/L; 30 °C; Fe/Ni dosage: 2.0 g/L; pH = 7.0 Fe–Ni ratio 5:1). As shown in Fig. 5, when Ni is used alone, 3-CCZ is hardly removed (5.1%). Using zero-valent iron alone, within 5 h, the removal rate only reached 80.3%. These data confirm the excellent removal characteristics of the bimetallic system. It confirmed that metal Ni not only acts as a catalyst to prevent the corrosion of Fe^0 and generate hydrogen through the reaction with water in the process of removing 3-CCZ, but also can reduce the corrosion and agglomeration of Fe^0 compared with using Fe^0 alone. The results also confirm previous research reports (Gao et al. 2016; Ying et al. 2016; Wu et al. 2017).

Kinetics of 3-CCZ removal by "Fe/Ni"

Reaction kinetics can be expressed conveniently as a pseudo-first-order reaction normalized to the surface area (Eq. 4). The rate constant (k_{obs}) and correlation coefficient (R^2) were calculated using Eq. (4) and Fig. 4d. The results are shown in Table 2. The data for the removal kinetics are in good agreement with a pseudo-first-order model due to the removal of 3-CCZ with $R^2 > 0.9$. The 3-CCZ's k_{obs} increased with increased temperature. It indicates that the increased temperature improves the removal rate of 3-CCZ (Liu et al. 2013).

Generally, the apparent activation energy E_a is calculated from the Arrhenius equation (Eq. 5) (Zhang et al. 2011). If focusing on the 3-CCZ removal mechanism, the apparent activation energy (E_a) needs to be considered (Carrier et al. 2016). If the values of E_a range from 8 to 21 kJ/mol, the reaction process is diffusion-controlled. If the activation energy is higher than 29 kJ/mol, it becomes a type of surface-controlled reaction (Lien and Zhang 2007). If the activation energy increases above 42.0 kJ/mol, it indicates that the rate determining step is surface limited (Chen et al. 2011). It means the higher the value of the activation energy is, the faster will be the removal rate. The E_a calculated for the removal of 3-CCZ is 112.7 kJ/mol. Thus, the 3-CCZ removal needs to be regarded as a surface-controlled reaction. On the basis of our kinetic studies, it can be concluded that the removal of 3-CCZ includes both adsorption and degradation.

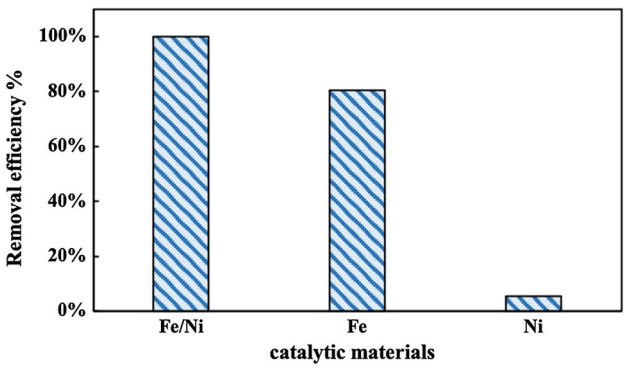

Fig. 5 Effect of different treatment processes on 3-CCZ removal efficiency. ($C_0 = 5$ mg/L; 30 °C; Fe/Ni dosage: 2.0 g/L; pH = 7.0 Fe–Ni ratio 5:1)

Table 2 Reaction temperature and removal parameter of 3-CCZ by "Fe/Ni"; conditions: 100 mL; $C_0 = 5$ mg/L; 30 °C; Fe/Ni dosage: 2.0 g/L; pH = 7.0

Temperature (°C)	k_{obs} (/h)	R^2
20	0.27	0.9957
30	1.91	0.960
35	2.07	0.954

Removal mechanism

The removal mechanism of organic pollutants such as 2,4-DCP and AMX by Fe/Ni has been investigated (Ruan et al. 2019; Weng et al. 2014a). The mechanism of Fe/Ni removal organic pollutant is that starting with an adsorption of the pollutant to "Fe/Ni" nanocomposites. Then, the catalytic reduction follows. To illustrate the removal mechanism of 3-CCZ by Fe/Ni nanocomposites, HPLC, microorganic analyses (CNS) and GC–MS were used for analysis in this study. In Table 2, data show that the removal of 3-CCZ fits well with a pseudo-first-order kinetic model.

The carbon mass percentage (C mass%), as shown in Table 3, is used as an indicator of the remaining carbon amount after surface adsorption of 3-CCZ to "Fe/Ni." The Fe/Ni background carbon mass before the reaction was 0.24%. After the reaction, its content has increased negligibly to 0.29%. It indicates that only a negligible amount of carbon had adsorbed on the Fe/Ni surface. These data show that there are two ways to remove 3-CCZ by Fe/Ni: adsorption on the Fe/Ni surface and catalytic reduction by Fe/Ni. Since only a negligible increase of the adsorbed carbon was detected, the reduction is likely to be the main process for removal of 3-CCZ.

Table 3 Elemental analysis of organic carbon before and after reaction

Sample	*C* mass%
Fe/Ni before reaction	0.24
Fe/Ni + 3-CCZ (after reaction)	0.29

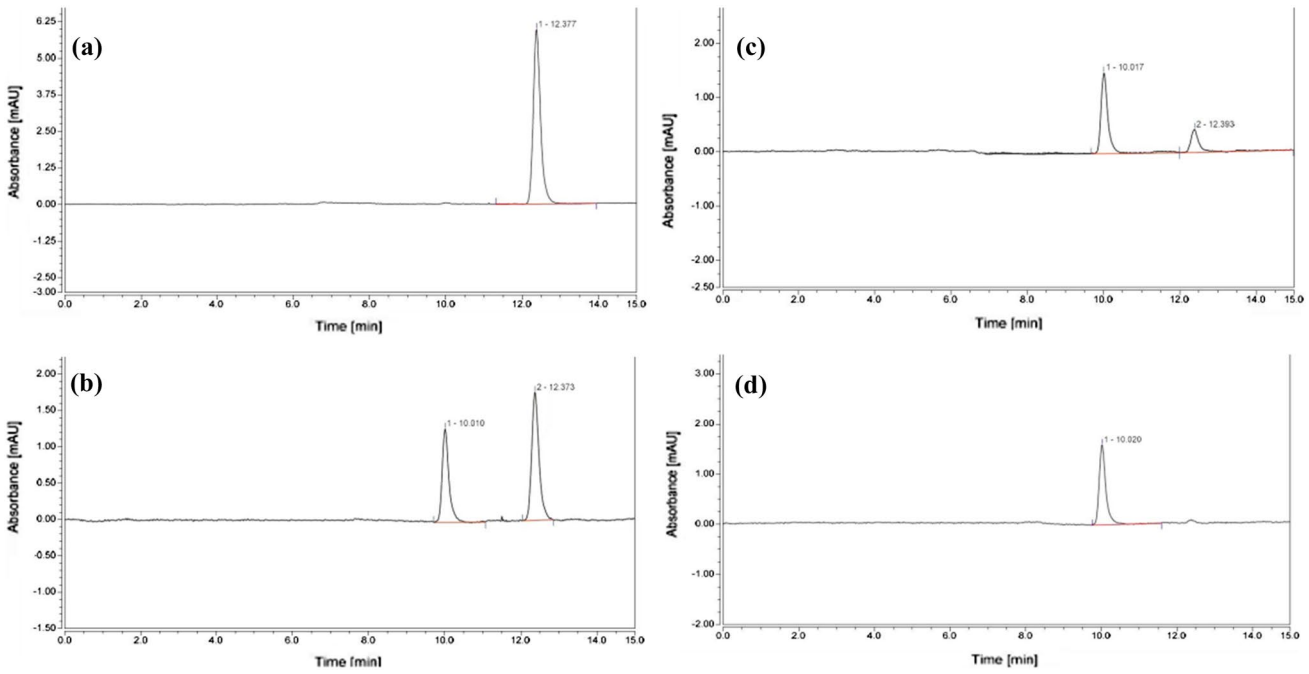

Fig. 6 HPLC diagrams of 3-CCZ degradation recorded at different reaction times. Conditions: 100 mL; C_0 = 5 mg/L; 30 °C; Fe/Ni dosage: 2.0 g/L; pH = 7.0. **a** 0 h; **b** 3 h; **c** 5 h; **d** 7 h

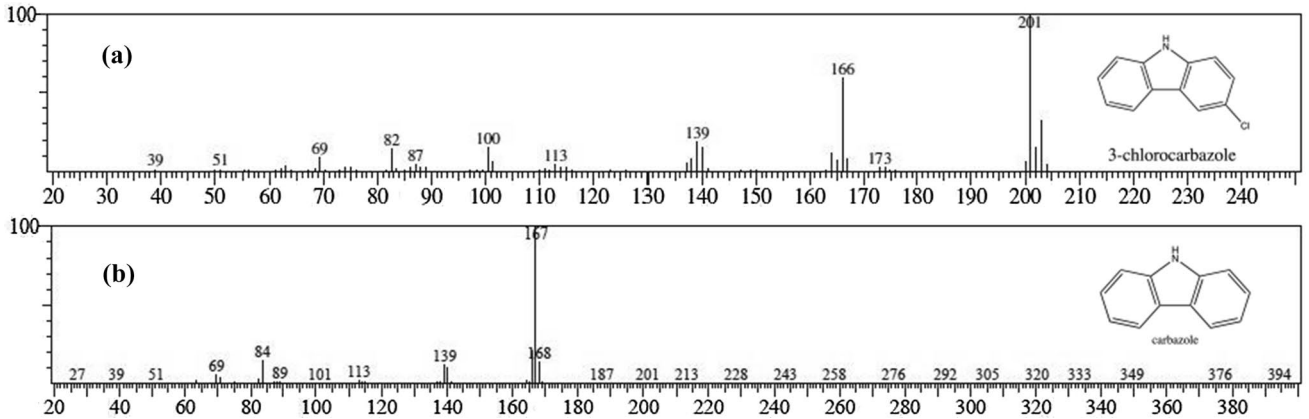

Fig. 7 GC–MS spectra of 3-CCZ **a** 3-CCZ before reaction **b** 3-CCZ after reaction

Figure 6 shows the peaks recorded by HPLC after a 3-CCZ reaction time of 0, 1, 3 and 5 h. At reaction time 0 h only a 3-CCZ peak at 12.3 min in the chromatogram appeared (Fig. 6a). An obvious product peak should have appeared at 10 min (Fig. 6b, c), as it occurred with prolonged reaction time. Only one product peak was visible after 5 h of reaction (Fig. 6d), indicating that 3-CCZ had been completely degraded. To analyze the degradation products of 3-CCZ, GC–MS analysis was applied to detect the structure of the products. Figure 7 shows the GC–MS mass spectra of 3-CCZ before and after the contact with "Fe/Ni." The resulting product is carbazole (m/z: 167.0). No other degradation product was detectable.

To further confirm the occurrence of dechlorination as a result of the removal 3-CCZ by Fe/Ni, the concentrations of Cl^- before and after the reaction were measured. The results are shown in Table 4. The data in Table 4 indicate that the concentration of Cl^{-1} increased from 1.3 to 2.0 mg/L within 1 h. After 3 h, the concentration of Cl^{-1} had increased to

Table 4 Cl^- concentrations during reaction

Time (/h)	Cl^- (mg/L)
0	1.3
1	2.1
3	4.7
5	4.9

4.7 mg/L. After 5 h, finally 4.9 mg/L were measured. The H· generated during the reaction breaks the C–Cl bond in the 3-CCZ molecule and in this way the concentration of Cl^{-1} increases. These results also indicate that most of the dechlorination of 3-CCZ occurs within the first 3 h. This is consistent with the results determined for the optimal reaction conditions (Fig. 4).

On the basis of the results above, the 3-CCZ removal pathway is described as follows (Eqs. (6–10)):

$$3-\mathrm{CCZ}+\mathrm{Fe/Ni}\ \rightarrow 3-\mathrm{CCZ}-\mathrm{Fe/Ni(adsorption)} \quad (6)$$

$$\mathrm{Fe^0}+2\mathrm{H^+}\rightarrow \mathrm{Fe^{2+}}+\mathrm{H_2} \quad (7)$$

$$2\mathrm{Ni^0}+\mathrm{H_2}\rightarrow 2\mathrm{Ni{-}H\bullet} \quad (8)$$

$$\mathrm{Ni{-}H}\rightarrow \mathrm{Ni^0}+\mathrm{H} \quad (9)$$

$$\mathrm{Ni{-}H}+\mathrm{CCZ}\rightarrow \mathrm{Ni}+\mathrm{carbazole}+\mathrm{H_2O}+\mathrm{Cl^{-1}} \quad (10)$$

The removal of 3-CCZ is divided into two steps: adsorption and reductive dechlorination. At first, the 3-CCZ molecules are adsorbed on the "Fe/Ni" surface (Eq. 6).

In the next step, the reduction by the nano-bimetallic "Fe/Ni" takes place. It involves the oxidation of Fe^0 and a formation of H_2 (Eq. 7). Then, the H_2 moves to the Ni^0 atoms on the surface resulting in the formation of nickel hydride (Ni–H) and finally H·radicals (Eqs. 8, 9) (Zou et al. 2016). The H· radicals attach 3-CCZ molecules, and 3-CCZ becomes dechlorinated and reduced to carbazole (m/z 167.0) and Cl^- (Eq. 10).

Taking all the results mentioned above into account, we propose a removal mechanism for 3-CCZ in combination with Fe/Ni as shown in Fig. 8. Once 3-CCZ is adsorbed on the Fe/Ni surface, the empty Ni orbital and p electrons form a transition complex with the *p*-electron pair of 3-CCZ or chlorine. This complexation reduces the activation energy of the dechlorination reaction. In addition, nickel metal as a hydrogenolysis catalyst can decompose H_2 generated by iron oxidation and produce H (Ruan et al. 2019). With these H radicals promote, 3-CCZ is degraded through the pathway shown in Fig. 8. H attacks the para-chlorine atom in the complex causing finally the generation of carbazole.

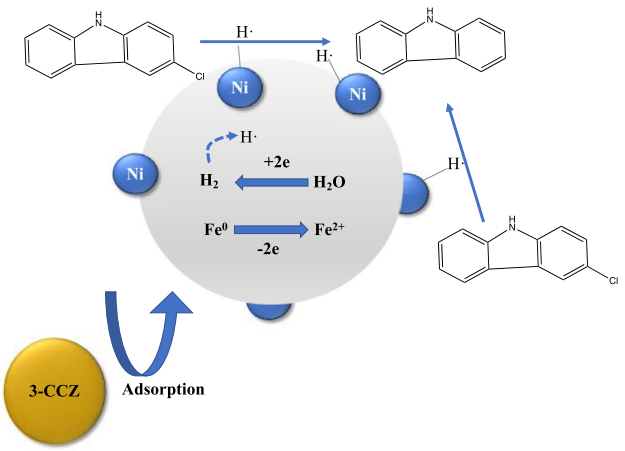

Fig. 8 Proposed removal mechanism for 3-CCZ by "Fe/Ni"

Conclusion

The results of this study have shown that Fe/Ni materials can effectively remove 3-CCZ. Ni acts as a catalyst to improve the reactivity of Fe. Secondly, degradation mechanism of 3-CCZ in water by the action of this catalyst is proposed. GC–MS analysis of the degradation products shows that the degradation process of 3-CCZ consists of adsorption followed by catalytic reduction. In addition, the pH of the solution, the amount of Fe/Ni, the ratio of Fe to Ni during material synthesis and the reaction temperature are the main factors affecting the removal efficiency. The kinetic study shows that the degradation conforms to a pseudo-first-order kinetic process. The calculation of E_a shows that the degradation process is a surface-controlled reaction. The removal of 3-CCZ from wastewater will be discussed further.

Authors' contribution All authors contributed to the study conception and design. Material preparation, data collection and analysis were performed by XK and DL. The first draft of the manuscript was written by XK, and all authors commented on previous versions of the manuscript. All authors read and approved the final manuscript. XK was involved in the conceptualization; DL and LC contributed to the methodology; XC and DL were involved in the formal analysis and investigation; XK was involved in writing—original draft preparation; XK and XZ contributed to the writing—review and editing; XZ, XC and XS acquired the funding; XZ contributed to the resources; XZ, XC and XS contributed to the supervision.

Funding The authors acknowledge the financial support from the Fundamental Research Funds for the Central Universities (Grant No. 2232019D3-21); the National Natural Science Foundation of China (Grant No. 51909034); the National Key Research and Development Program of China (No. 2019YFC0408603); the Shanghai Sailing Program (Grant No. 19YF1401900). This project is also supported by the special fund from the Hubei Provincial Engineering Research Center of Systematic Water Pollution Control (China University of Geosciences, Wuhan, P.R. China) (Project No. 20190813); the National Key Research and Development Project (Grant No.2019YFC0408604);

Research project of ecological environment protection and restoration of Yangtze River in Zhoushan (SZGXZS2020068).

Data availability and materials All data generated or analyzed during this study are included in this published article [and its supplementary information files].

Declarations

Conflict of interest The authors declare that they have no conflict of interest.

References

Bokare AD, Chikate RC, Rode CV, Paknikar KM (2008) Iron–nickel bimetallic nanoparticles for reductive degradation of azo dye orange G in aqueous solution. Appl Catal B-Environ 79:270–278

Carrier M, Auret L, Bridgwater A, Knoetze JH (2016) Using apparent activation energy as a reactivity criterion for biomass pyrolysis. Energy Fuels 30:7834–7841

Chen ZX, Jin XY, Chen Z, Megharaj M, Naidu R (2011) Removal of methyl orange from aqueous solution using bentonite-supported nanoscale zero-valent iron. J Colloid Interface Sci 363:601–607

Cheng L et al (2021) Preparation and piezoelectric catalytic performance of HT-Bi2MoO6 microspheres for dye degradation. Adv Powder Technol 32:3346–3354

Dong T, Luo H, Wang Y, Hu B (2011) Stabilization of Fe–Pd bimetallic nanoparticles with sodium carboxymethyl cellulose for catalytic reduction of para-nitrochlorobenzene in water. Desalination 271(1-3):11–19

Ezzatahmadi N, Ayoko GA, Millar GJ, Speight R, Yan C, Li J, Li S, Zhu J, Xi Y (2016) Clay-supported nanoscale zero-valent iron composite materials for the remediation of contaminated aqueous solutions: a review. Chem Eng J 312:336–350

Ezzatahmadi N, Marshall DL, Hou K, Ayoko GA, Millar GJ, Xi Y (2019) Simultaneous adsorption and degradation of 2,4-dichlorophenol on sepiolite-supported bimetallic Fe/Ni nanoparticles. J Environ Chem Eng 7(2):102955

Fang Z, Qiu X, Chen J, Qiu X (2011) Debromination of polybrominated diphenyl ethers by Ni/Fe bimetallic nanoparticles: influencing factors, kinetics, and mechanism. J Hazard Mater 185:958–969

Feng Z et al (2020) In situ preparation of g-C3N4/Bi4O5I2 complex and its elevated photoactivity in methyl orange degradation under visible light. J Environ Sci 87:149–162

Fu F, Dionysiou DD, Liu H (2014) The use of zero-valent iron for groundwater remediation and wastewater treatment: a review. J Hazard Mater 267:194–205

Gao Y et al (2016) Comparison of degradation mechanisms of microcystin-LR using nanoscale zero-valent iron (nZVI) and bimetallic Fe/Ni and Fe/Pd nanoparticles. Chem Eng J 285:459–466

Ghauch A, Tuqan A, Assi HA (2009) Antibiotic removal from water: elimination of amoxicillin and ampicillin by microscale and nanoscale iron particles. Environ Pollut 157:1626–1635

Li Z et al (2020a) Distribution characteristics and risk assessment of polyhalogenated carbazoles in sea water of the Yellow Sea. Mar Pollut Bull 161:111656

Li Z, Fan X, Mu Y, Wang L, Liang J, Deng L (2020a) Distribution characteristics and risk assessment of polyhalogenated carbazoles in sea water of the Yellow Sea. Mar Pollut Bull 161:111656

Lien HL, Zhang WX (2007) Nanoscale Pd/Fe bimetallic particles: catalytic effects of palladium on hydrodechlorination. Appl Catal B-Environ 77:110–116

Lin Y, Chen Z, Megharaj M, Naidu R (2012) Degradation of scarlet 4BS in aqueous solution using bimetallic Fe/Ni nanoparticles. J Colloid Interface Sci 381:30–35

Liu X, Chen Z, Chen Z, Megharaj M, Naidu R (2013) Remediation of direct black G in wastewater using kaolin-supported bimetallic Fe/Ni nanoparticles. Chem Eng J 223:764–771

Lu CA et al (2021) High piezo/photocatalytic efficiency of Ag/Bi 5O7I nanocomposite using mechanical and solar energy for N2 fixation and methyl orange degradation. Green Energy Environ. https://doi.org/10.1016/j.gee.2021.04.009

Ma Y, Li Z, Yuan M, Chen L, Zhou S (2017) Isolation and identification of 3-bromocarbazole-degrading bacteria. J Environ Health B 52(11):796–801

Mukherjee R, Kumar R, Sinha A, Lama Y, Saha AK (2011) A review on synthesis, characterization and applications of nano-zero valent iron (nZVI) for environmental remediation. Crit Rev Environ Sci Technol 35:360–365

Nidheesh PV, Gandhimathi R (2012) Trends in electro-Fenton process for water and wastewater treatment: an overview. Desalination 299:1–15

Pan X, Li C, Chen J, Liu J, Li A (2019) The photodegradation of 1,3,6,8-tetrabromocarbazole in n-hexane and in solid-mediated aqueous system: kinetics and transformation mechanisms. Chem Eng J 375:121986

Qiu Y, Liu K, Zhou S, Chen D, Wang Y (2019a) Polyhalogenated carbazoles in surface sediment from Sanmen Bay, East China Sea: spatial distribution and congener profile. Bull Environ Contam Toxicol 103(1):41–47

Qiu Y, Zheng M, Wang L, Zhao Q, Qu L (2019b) Sorption of polyhalogenated carbazoles (PHCs) to microplastics. Mar Pollut Bull 146:718–728

Ruan X, Liu H, Wang J, Zhao D, Fan X (2019) A new insight into the main mechanism of 2,4-dichlorophenol dechlorination by Fe/Ni nanoparticles. Sci Total Environ 697:133996.1-133996.8

Shanshan Z, Xiaoxue P, Qiaozhi T, Hongbin Z, Jiayi Z (2019) Photochemical degradation of polyhalogenated carbazoles in hexane by sunlight. Sci Total Environ 671:622–631

Su J, Lin S, Chen Z, Megharaj M, Naidu R (2011) Dechlorination of p-chlorophenol from aqueous solution using bentonite supported Fe/Pd nanoparticles: synthesis, characterization and kinetics. Desalination 280:167–173

Theron J et al (2008) Nanotechnology and water treatment: applications and emerging. Crit Rev Microbiol 34:43–69

Wang G et al (2019) New insight into the formation of polyhalogenated carbazoles: aqueous chlorination of residual carbazole under bromide condition in drinking water. Water Res 159:252–261

Weng X, Chen Z, Chen Z, Megharaj M, Naidu R (2014a) Clay supported bimetallic Fe/Ni nanoparticles used for reductive degradation of amoxicillin in aqueous solution: characterization and kinetics. Colloid Surf A Physicochem Eng Asp 443:404–409

Weng X, Sun Q, Lin S, Chen Z, Megharaj M, Naidu R (2014b) Enhancement of catalytic degradation of amoxicillin in aqueous solution using clay supported bimetallic Fe/Ni nanoparticles. Chemosphere 103:80–85

Wu Y, Tan H, Sutton R, Chen D (2017) From sediment to top predators: broad exposure of polyhalogenated carbazoles in San Francisco Bay (USA). Environ Sci Technol 51:2038

Wu Y, Tan H, Zhou C, Crimmins BS, Holsen TM, Chen D (2018) Bioaccumulation and spatiotemporal trends of polyhalogenated carbazoles in Great Lakes fish from 2004 to 2016. Environ Sci Technol 52(8):4536–4545

Xi Y, Sun Z, Hreid T, Ayoko GA, Frost RL (2014) Bisphenol A degradation enhanced by air bubbles via advanced oxidation using in situ generated ferrous ions from nano zero-valent iron/palygorskite composite materials. Chem Eng J 247:66–74

Xiaojun Z, Minggang Z, Xiaocai Y, Ling W, Yinghua L (2019) Sorption of 3,6-dibromocarbazole and 1,3,6,8-tetrabromocarbazole by microplastics. Mar Pollut Bull 138:458–463

Yin W, Wu J, Li P, Wang X, Zhu N, Wu P, Yang B (2012) Experimental study of zero-valent iron induced nitrobenzene reduction in groundwater: the effects of pH, iron dosage, oxygen and common dissolved anions. Chem Eng J 184:198–204

Ying L et al (2016) Catalytic debromination of tetrabromobisphenol A by Ni/nZVI bimetallic particles. Chem Eng J 284:1242–1250

Zhang Z, Cissoko N, Wo J, Xu X (2009) Factors influencing the dechlorination of 2,4-dichlorophenol by Ni-Fe nanoparticles in the presence of humic acid. J Hazard Mater 165:78–86

Zhang X, Lin S, Chen Z, Megharaj M, Naidu R (2011) Kaolinite-supported nanoscale zero-valent iron for removal of Pb2+ from aqueous solution: reactivity, characterization and mechanism. Water Res 45:3481–3488

Zhao D, Cheng J, Chen J (2014) One-step synthesis of bentonite-supported nanoscale Fe/Ni bimetals for rapid degradation of methyl orange in water. Environ Chem Lett 12:461–466

Zhou T, Li Y, Lim TT (2010) Catalytic hydrodechlorination of chlorophenols by Pd/Fe nanoparticles: comparisons with other bimetallic systems, kinetics and mechanism. Sep Purif Technol 76:206–214

Zhou W, Chen W, Li P, Gu Z, Peng J, Lin K (2020) Occurrence and distribution of polyhalogenated carbazoles (PHCs) in sediments from the northern South China Sea. Sci Total Environ 753:142072

Zhu L, Hites RA (2006) Identification of brominated carbazoles in sediment cores from Lake Michigan. Environ Sci Technol 39:9446–9451

Zou Y, Wang X, Khan A, Wang P, Liu Y, Alsaedi A, Hayat T, Wang X (2016) Environmental remediation and application of nanoscale zero-valent iron and its composites for the removal of heavy metal ions: a review. Environ Sci Technol 50:7290–7304

Authors and Affiliations

X. Kang[1] · D. Li[2] · L. Chu[3] · X. Zhao[1] · X. Song[4] · X. Cao[5,6]

[1] Textile Pollution Controlling Engineering Center of Ministry of Environmental Protection, College of Environmental Science and Engineering, Donghua University, Rm. 5153, Bldg. 4, 2999 Renmin North Road, Songjiang District, Shanghai 201620, People's Republic of China

[2] Textile Pollution Controlling Engineering Center of Ministry of Environmental Protection, College of Environmental Science and Engineering, Donghua University, Rm. 5159, Bldg. 4, 2999 Renmin North Road, Songjiang District, Shanghai 201620, People's Republic of China

[3] Textile Pollution Controlling Engineering Center of Ministry of Environmental Protection, College of Environmental Science and Engineering, Donghua University, Rm. 5159, Bldg. 4, 2999 Renmin North Road, Songjiang District, Shanghai 201620, People's Republic of China

[4] Textile Pollution Controlling Engineering Center of Ministry of Environmental Protection, College of Environmental Science and Engineering, Donghua University, Shanghai 201620, People's Republic of China

[5] Textile Pollution Controlling Engineering Center of Ministry of Environmental Protection, College of Environmental Science and Engineering, Donghua University, Rm. 5153, Bldg. 4, 2999 Renmin North Road, Songjiang District, Shanghai 201620, People's Republic of China

[6] Shanghai Institute of Pollution Control and Ecological Security, Shanghai 200092, People's Republic of China